II06

Poster #0518

THE PROPERTIES AND SOURCES OF GRAVITY WAVES DETECTED BY THE TIDDBIT SOUNDER NEAR WALLOPS ISLAND ON 30 OCTOBER, 2007

Sharon L. Vadas
vasha@cora.nwra.com
NorthWest Research Associates, CoRA div., 3380 Mitchell Lane, Boulder, CO, 80503, USA

Geoff Crowley
gcrowley@astraspace.net
Atmospheric & Space Technology Research Associates, San Antonio, TX, 78249, USA

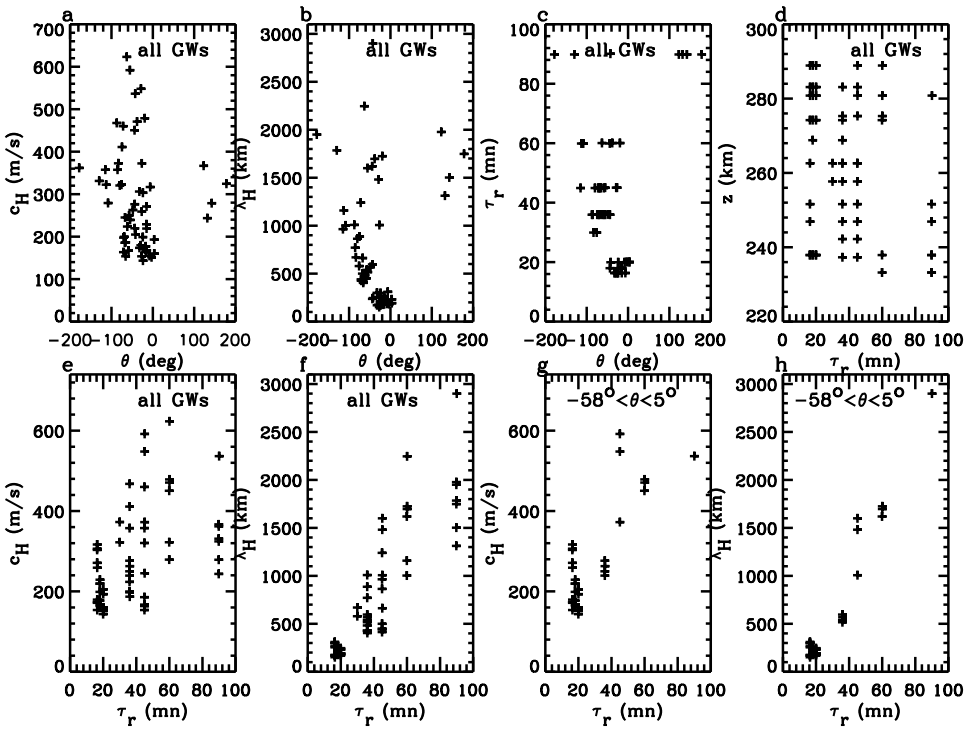

Figure 1: Attributes of GWs observed by TIDDBIT from 04:00-07:00 UT on October 30. Each "+" denotes a GW. a)-f) All 59 GWs. g)-h) Only those 36 GWs with azimuths of $-58^o < \theta < 5^o$. c_H is horizontal phase speed, λ_H is horizontal wavelength, τ_r is observed period, z is the reflection height. From Vadas and Crowley (2009).

TIDDBIT sounder waves at bottomside of F layer

• Waves were observed near Wallops Island on 30 October, 2007, using a new Doppler radar system called TIDDBIT which utilizes three transmitters and one receiver to measure the propagation characteristics of travelling ionospheric disturbances (TIDs) in the bottomside F-region of the ionosphere (Crowley *et al.*, 2009). Only those waves with observed periods of $15 < \tau_r < 90$ min are analyzed in this study.

• Fig. 1 shows that waves were propagating in nearly all directions, although most were propagating northwest(NW)ward. All GWs had $c_H > 100$ m/s and $\lambda_H > 100$ km at the reflection altitudes of $z = 230 - 290$ km, consistent with dissipative GW theory (Vadas, 2007; Fritts and Vadas, 2008). Those medium-scale waves with horizontal wavelengths of $100 < \lambda_H < 400$ km had the smallest periods of $15 < \tau_r < 30$ min.

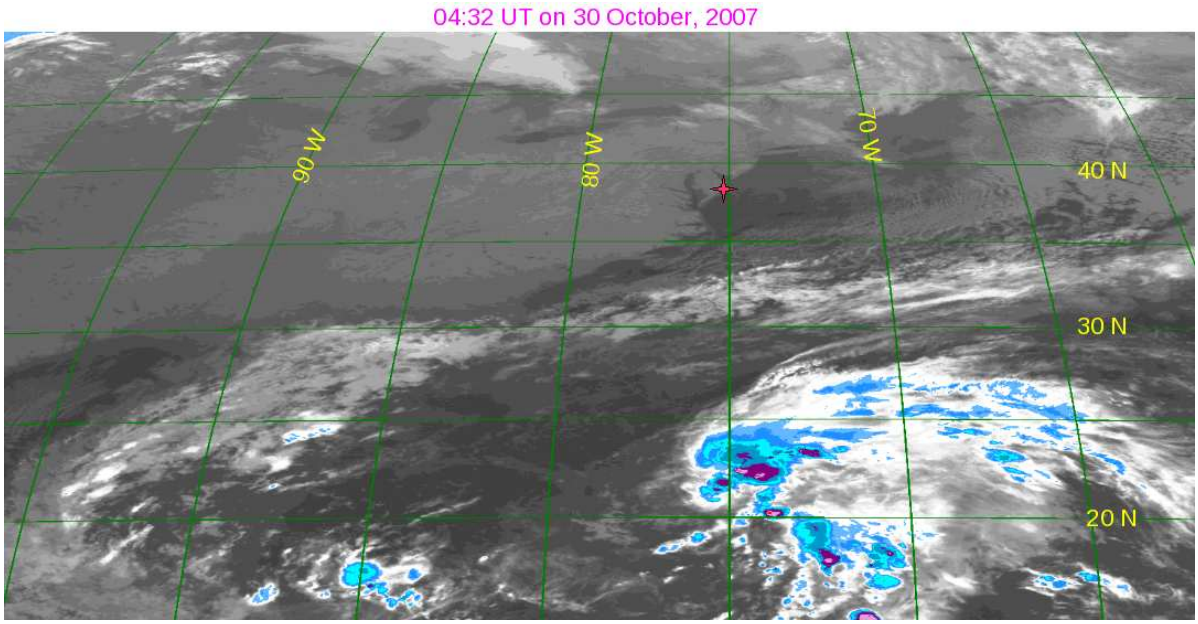

Figure 2: GOES satellite image on October 30 at 04:32 UT. The temperature of the tropopause (where convective plumes need to reach in order to excite GWs) is estimated to be $\sim -79^{o}$ C. The transition from white to blue occurs at -55^{o} C. The dark purple color denotes -75 to -80^{o} C. The plum and red colors denote fluids colder than -80^{o} C, where GWs were likely excited. Wallops Island is shown by the red star at 75.47^{o} W and 37.95^{o} N. From Vadas and Crowley (2009).

GOES satellite image of the mid Atlantic american coast

• At the time of the observations, Tropical Storm (TS) Noel was located $\sim$ 2000 km southeast (SE) of Wallops Island. Noel began as a TS on 28 October, and turned into a hurricane on 02 November. By 03 November, it began to dissipate as it reached the cold water off the Eastern Coast of North America. It subsequently moved NEwards up the east coast of North America, and dissipated by 06 November near 50^{o} W and 64.2^{o} N.

• Fig. 2 shows a satellite image color-coded for temperature. Those purple and red colors denote deep convective plumes and clusters which generated GWs. Some of those clusters were very intense, with updraft velocities of up to $\sim$ 75 m/s. Note that the band of white clouds between Noel and the east coast is an area of weak convection and high cirrus clouds that was much warmer than the tropopause, and therefore did not likely excite GWs.

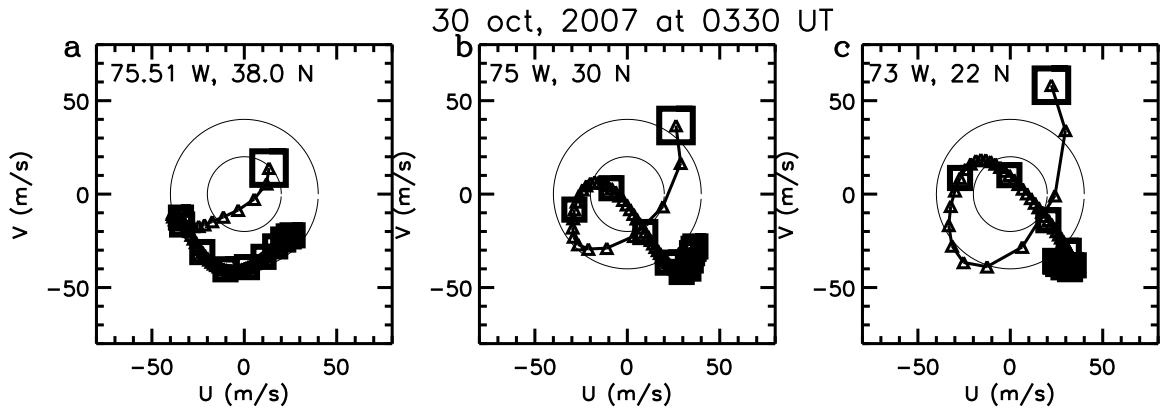

Figure 3: Hodograph of the background horizontal wind from $z = 100$ to 300 km at 03:30 UT from the TIME-GCM. Triangles are every 2 km in altitude, the large square denotes the wind at $z = 100$ km, and medium-sized squares indicate the winds every 20 km. a) 75.51° W and 38.0° N. b) 75° W and 30° N. c) 73° W and 22° N. From Vadas and Crowley (2009).

Background thermospheric winds near Wallops Island

• Fig. 3 shows hodographs of the neutral thermospheric winds. These winds were generally to the S and SW in the lower thermosphere, thereby favoring northward and NEward propagation of the primary GWs excited by TS Noel.

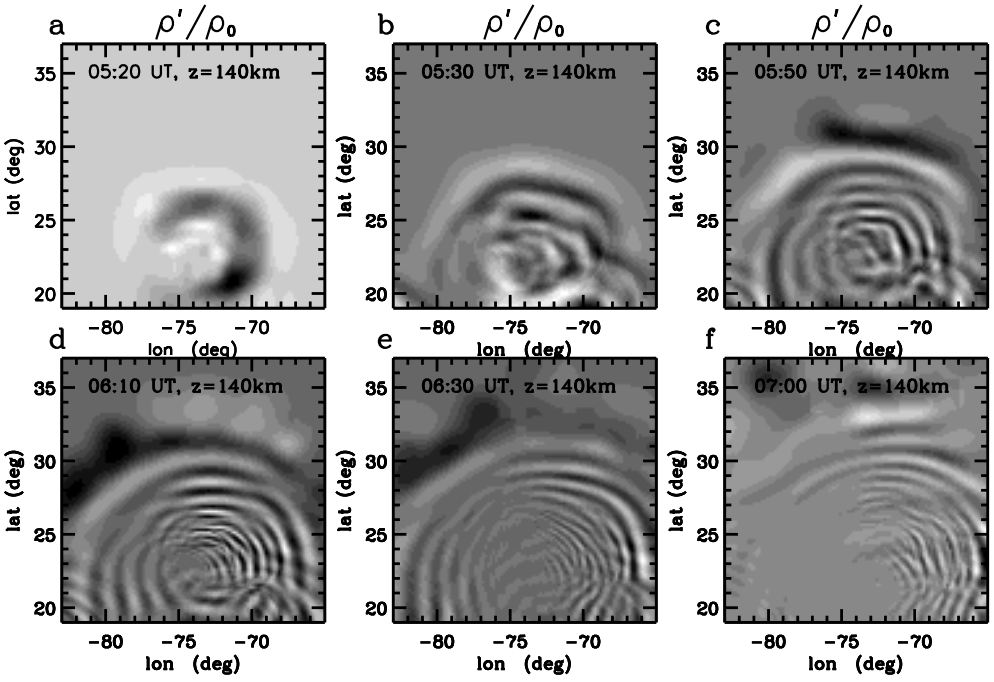

Figure 4: Horizontal slices of $\rho'/\overline{\rho}$ at $z = 140$ km as a function of time. a)-f) shows the slices at 05:20, 05:30, 05:50, 06:10, 06:30, and 07:00 UT. The maximum values of $\rho'/\overline{\rho}$ are (a-c): 34, 18, and 23%. (d-f): 23, 23, and 17%. From Vadas and Crowley (2009).

Density perturbations of primary GWs

• Fig. 4 shows the GW density perturbations, $\rho'/\overline{\rho}$, at $z = 140$ km as a function of time from 05:20 to 07:00 UT. These GWs are excited by the 15 convective objects undergoing convective overshoot in Fig. 2. Here, the ray tracing includes parameterized GW breaking via Lindzen's linear saturation scheme (Lindzen, 1981). Distorted concentric rings are observed. Constructive and destructive interference patterns from the GWs from different clusters are also seen.

• At early times, large λ_H waves propagate to this altitude. At later times, relatively smaller λ_H waves propagate to this altitude, since they have smaller vertical group velocities.

• The maximum density perturbations are $\sim 35\%$ (50 min after GW excitation), but are typically 20-25%. This corresponds to GW horizontal wind perturbation amplitudes of $\sim 200 - 300$ m/s (Vadas *et al.*, 2009).

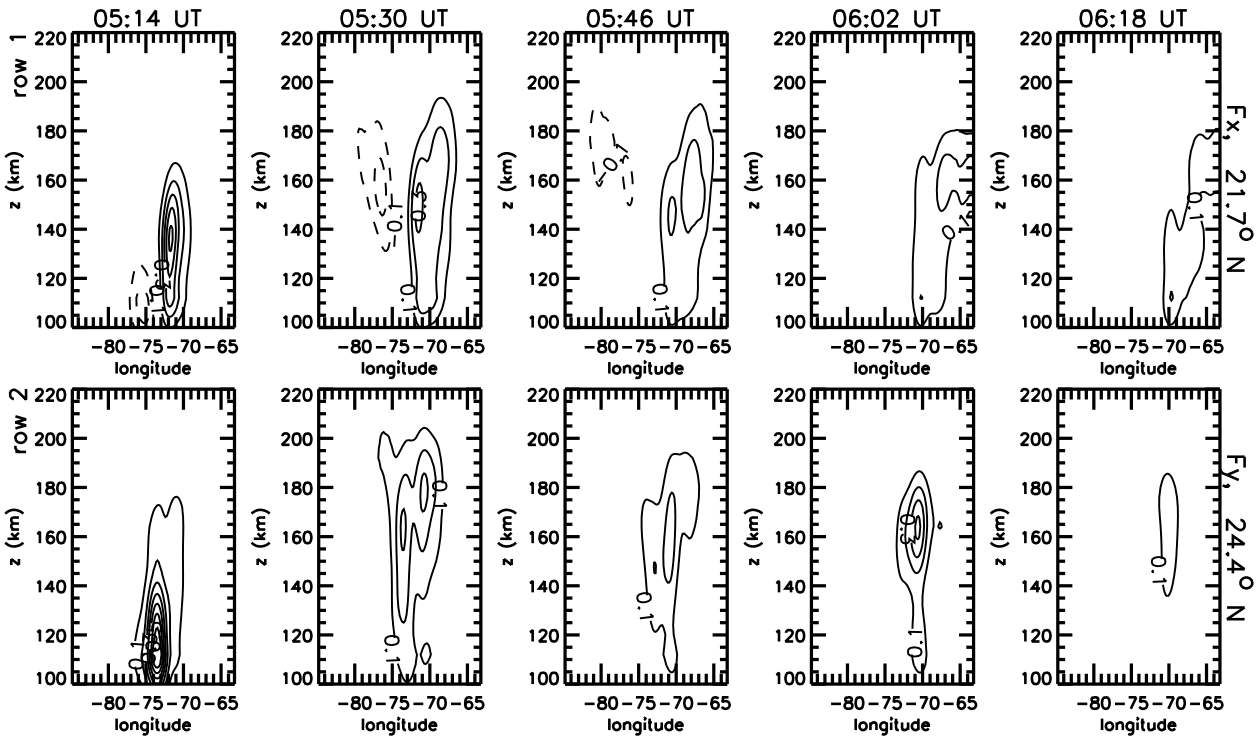

Figure 5: Thermospheric body forces as a function of longitude and altitude calculated from the GWs excited from all convective objects in intervals of 0.1 m s^{-2}. Solid lines indicate positive values, and dashed lines indicate negative values. Row 1: Zonal acceleration at 21.7° N. Row 2: Meridional acceleration at 24.4° N. The first, second, third, forth, and fifth times in each row correspond to 05:14, 05:30, 05:46, 06:02, and 06:18 UT, respectively. The maximum zonal forcing is eastward, with a value of 0.61 m s^{-2}, at 71.7° W and 21.7° N and 05:20 UT. The maximum meridional forcing is northward, with a value of 0.85 m s^{-2}, at 73.5° W, 24.4° N and 05:14 UT. From Vadas and Crowley (2009).

Thermospheric body forces created from the dissipation of GWs from Noel

- Fig. 5 shows the thermospheric body forces calculated after forward ray tracing the GWs excited by the deep convective plumes in Fig. 2. As expected, the body forces are primarily northward and eastward. The northward forcing has a maximum value of ~ 0.9 m/s^2.

- The body forces range in altitude from $z \sim 110$ to 190 km.

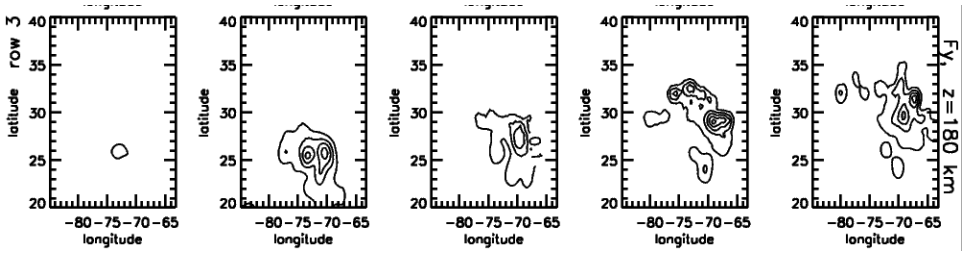

Figure 6: Horizontal slices of the northward component of the body force calculated from all convective objects at $z = 180$ km and at 05:14, 05:30, 05:46, 06:02, and 06:18 UT from left to right, respectively. Solid contours are in intervals of 0.1 m s^{-2}. From Vadas and Crowley (2009).

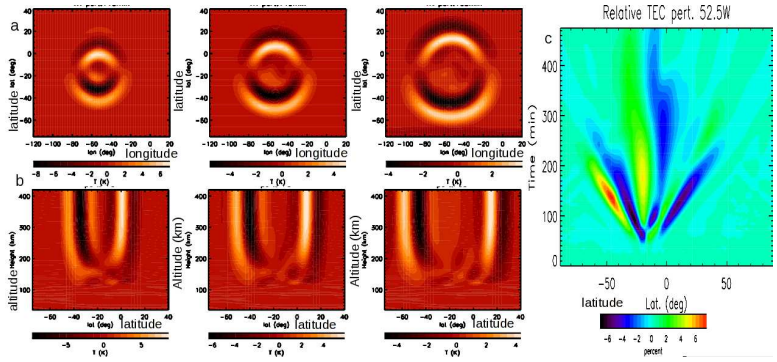

Figure 7: a) Time series of horizontal slices of the difference temperature perturbations, T' (in degrees K), at $z = 250$ km induced from a thermospheric body force at 53.2°W and 17.7°S. From left to right, $\Delta\mathcal{T} = 115$, 140, and 165 min. The body force begins at $\Delta\mathcal{T} = 24$ min, and is maximum at $\Delta\mathcal{T} = 45$ min. b) Same as in a), but latitude-altitude slices of T' at 52.5°W. c) Difference total electron content (TEC) (in %) at 52.5°W as a function of latitude and time. From Vadas and Liu (2009).

Meridional component of created thermospheric body forces

• Fig. 6 shows that the approximate horizontal regions occupied by thermospheric body forces is $62 - 80^o$ W, and $20 - 33^o$ N. This region moves northward with time.

• Fig. 7 shows that upward and downward-propagating secondary GWs are excited by thermospheric body forces. Note that those downward-propagating GWs reflect upwards at $z \sim 120$ km. This TIME-GCM study was performed for a deep convective plume in Brazil, and is resolution limited to $\lambda_H > 2000$ km. Thus, medium-scale secondary GWs are not resolved in that study.

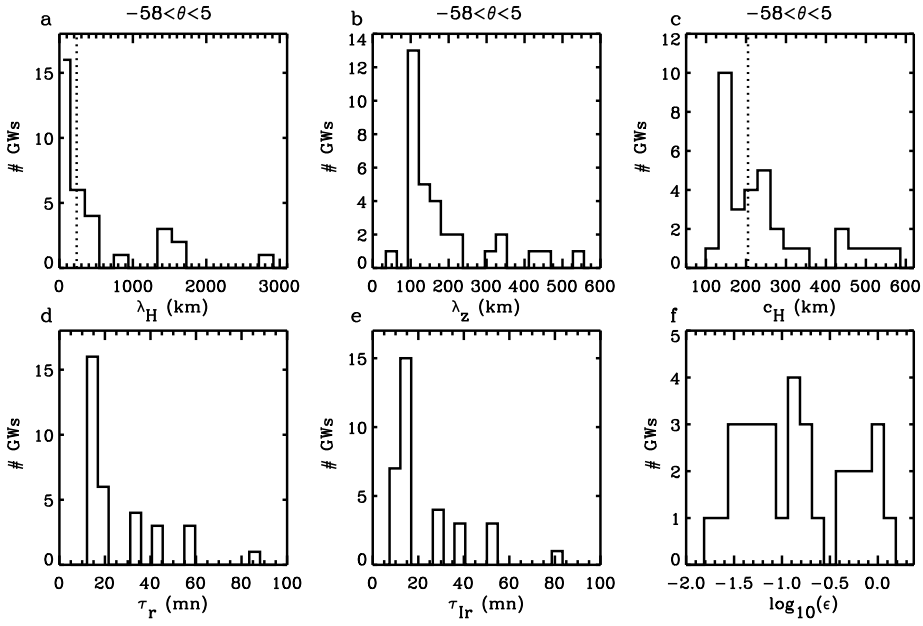

Figure 8: Histograms of the numbers of GWs as a function of λ_H, λ_z, c_H, τ_r, intrinsic frequency τ_{Ir}, and $\log_{10}(\epsilon)$ for the GWs with $-58^o \leq \theta \leq 5^o$. Here, ϵ is the dissipation factor, given by Eq. (0.1). The dotted lines show $c_H = 205$ m/s and $\lambda_H = 235$ km. From Vadas and Crowley (2009).

Distribution of TIDDBIT sounder waves from 04:00-10:00 UT

• Fig. 8 shows the distributions of N/NWward propagating waves. Most waves had horizontal wavelengths of $\lambda_H = 100 - 500$ km and horizontal phase speeds of $c_H = 100 - 300$ km, although a few had horizontal wavelengths as large as $\lambda_H = 1000 - 3000$ km.

• The dissipation factor, ϵ, is

$$\epsilon = \frac{|k_H m| N}{\mathrm{H}(\mathbf{k}^2 + 1/4\mathrm{H}^2)^{3/2}|\mathbf{k}^2 - 1/4\mathrm{H}^2|(1 + \mathrm{Pr}^{-1})\nu}. \tag{0.1}$$

Here, $\epsilon \simeq 1$ when a GW's momentum flux is maximum (i.e., at $z = z_{\rm diss}$), $\epsilon \gg 1$ when a wave is not yet dissipating, and $\epsilon \ll 1$ when a wave is strongly dissipating. At the reflection altitude, GW dissipative theory predicts that $\lambda_H > 100$ km, $c_H > 100$ m/s, $10 < \tau_{Ir} < 90$ min, and $\log_{10}(\epsilon) \geq -2.1$. Therefore, Fig. 8 shows that the wave parameters measured by TIDDBIT agree well with GW dissipative theory (Vadas, 2007; Fritts and Vadas, 2008).

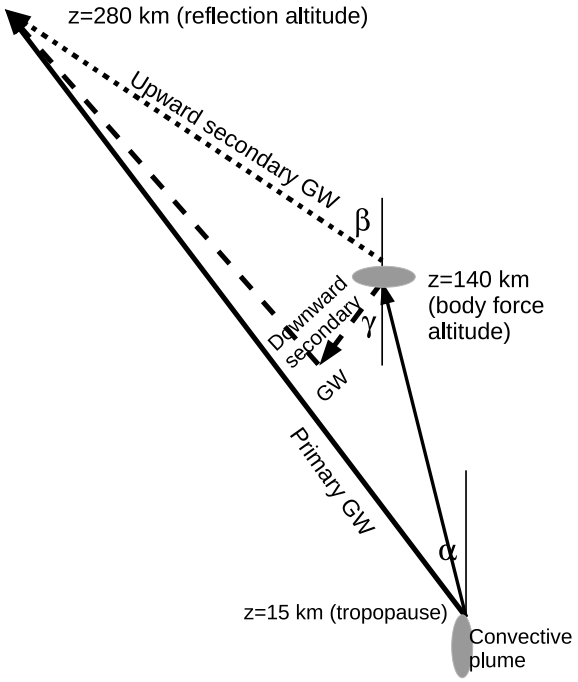

Figure 9: Sketch of the tropospheric and thermospheric sources of GWs considered here. The convective plume excites primary GWs (black lines). Those which have larger λ_H propagate up to the reflection altitude, while those with smaller λ_H dissipate at $z \sim 140$ km, creating a thermospheric body force (grey ellipse). Upward (dot line) and downward (dash lines) propagating secondary GWs are excited by the thermospheric body force. Those initially downward-propagating secondary GWs reflect upwards in the upper mesosphere or lower thermosphere. Both propagate to the reflection altitude. From Vadas and Crowley (2009).

Possible source geometries in troposphere and thermosphere

• Fig. 9 shows a sketch of the wave sources we consider here. Here, we choose the tropopause as a possible excitation source, because active, deep convection was occurring in TS Noel (see Fig. 2). NCEP reanalysis shows that the tropopause was at $z_{\rm trop} = 15.0$ km near TS Noel.

• We also choose the thermosphere as a possible excitation source, because secondary GWs are excited in the thermosphere after the small-scale primary convective GWs dissipate (see Fig. 5-7). We choose $z \sim 140$ km because that is the "average" altitude of the thermospheric body forces (see Fig. 5). Because the primary and secondary GWs are excited as both upward and downward propagating GWs (see Fig. 7), we include reflection in our reverse ray tracing.

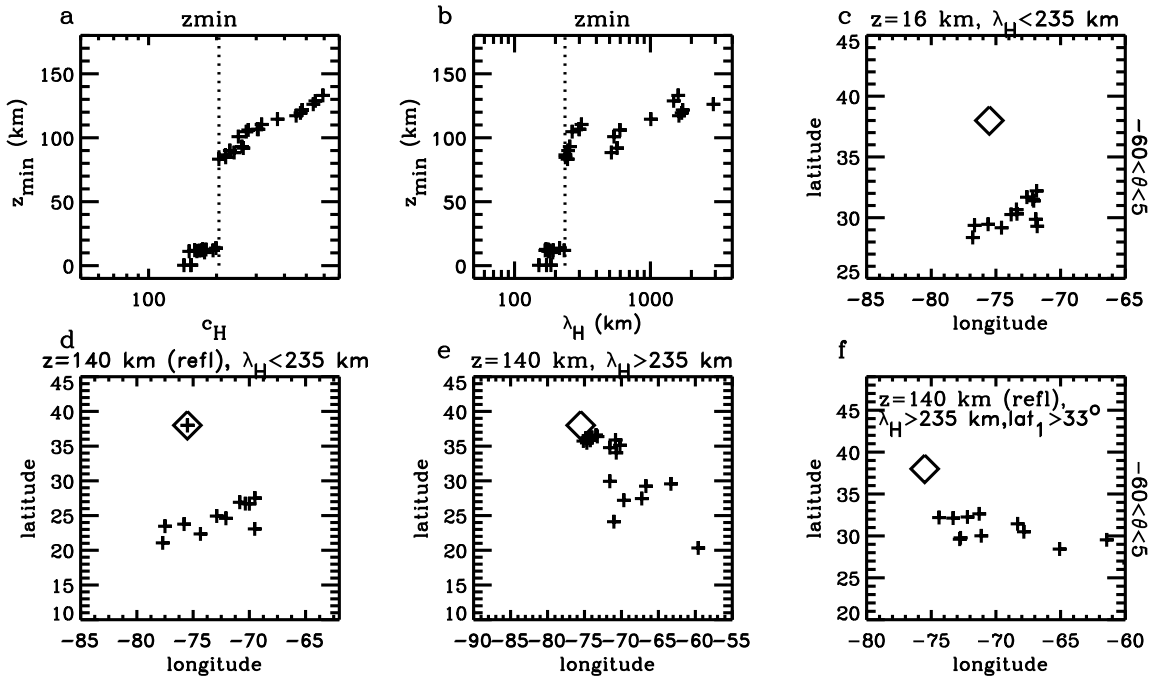

Figure 10: Reverse ray trace results using the model horizontal background winds from the TIME-GCM only for the 33 GWs propagating N/NWward. a) The minimum altitude, $z_{\min}$, as a function of c_H. The dotted line shows $c_H = 205$ m/s. b) $z_{\min}$ as a function of λ_H. The dotted line shows $\lambda_H = 235$ km. c) Locations of the GWs which reverse ray-traced to $z = 16$ km. d) Locations of the GWs with $\lambda_H < 235$ km at $z = 140$ km after having reflected once. e) Locations of the GWs with $\lambda_H > 235$ km at $z = 140$ km just below the observation altitude. f) Locations of the GWs with $\lambda_H > 235$ km at $z = 140$ km after having reflected once, but only including those GWs N of 33° in e). From Vadas and Crowley (2009).

Source locations for N/NWward propagating waves

• We reverse ray trace all N/NWward-propagating GWs with $-58^o \leq \theta \leq 5^o$. Fig. 10a-b shows that only GWs with $c_H < 205$ m/s and $\lambda_H < 235$ km can propagate from the tropopause. All other waves can propagate no lower than $80 - 140$ km.

• Fig. 10c shows the reverse ray-traced "touchdown" locations at $z = 16$ km of those observed waves with $c_H < 205$ m/s and $\lambda_H < 235$ km. These touchdown locations occur at $28 - 33^o$ N, which is ~ 500 km north of any deep convective sources in Fig. 2. Therefore, those GWs with $c_H < 205$ m/s and $\lambda_H < 235$ km were likely not primary convective waves. This is not surprising, since Noel was 2000 km away, and primary waves with

periods of $15 - 25$ min propagate to $z \sim 250$ km after travelling only $\sim 750 - 1250$ km horizontally. (e.g., Hines, 1967; Waldock and Jones, 1987). GWs with larger periods travel further horizontally while attaining the same altitude.

• We continued reverse ray-tracing the medium-scale GWs with $\lambda_H <$ 235 km backwards in time to a possible thermospheric body force. Fig. 10d shows the possible locations of the sources at $z \simeq 140$ km. We see that they occur at $65 - 80^o$ W and $20 - 30^o$ N. This region matches the body force source region shown in Fig. 6 very well. Therefore, the GWs with $c_H <$ 205 m/s and $\lambda_H < 235$ km were likely initially downward-propagating secondary GWs from thermospheric body forces created from TS Noel.

• Fig. 10e and f shows that those GWs with $\lambda_H > 235$ km are likely a mixture of initially upward and downward propagating secondary GWs from the thermospheric body forces.

• Of the 33 NW/Nward waves, we identified 27 as secondary GWs from TS Noel. None were identified as primary GWs. Altogether, 21 of the waves were identified as likely initially downgoing, while 6 were identified as likely initially upgoing secondary GWs.

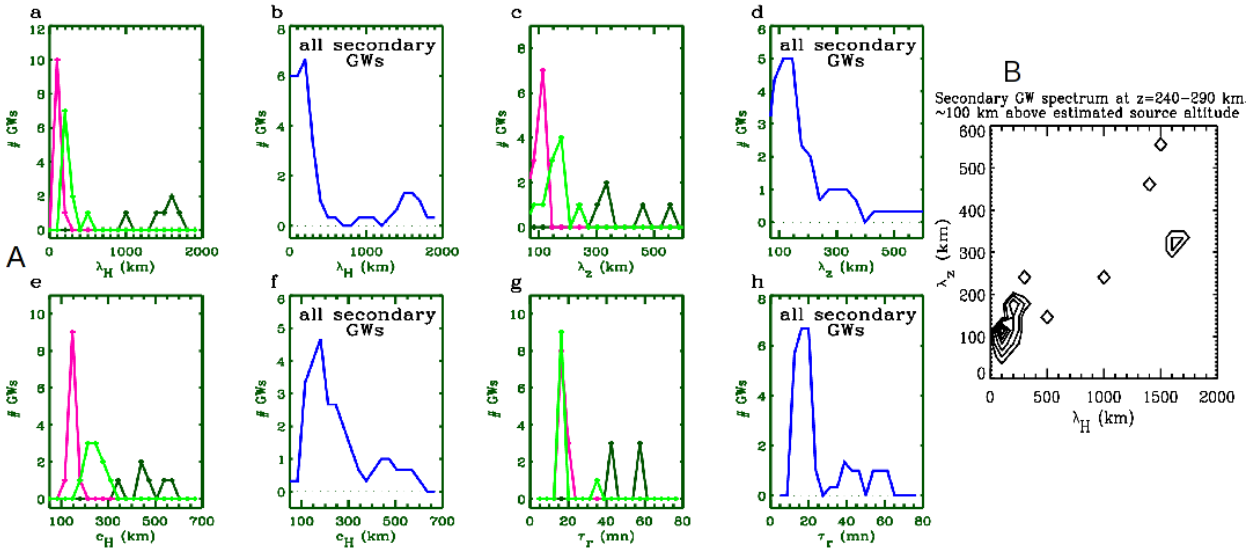

Figure 11: Panel A: Numbers of secondary GWs (identified from reverse ray tracing) as a function of λ_H (a-b), λ_z (c-d), c_H (e-f), and τ_r (g-h) for the GWs with $-58^o \leq \theta \leq 5^o$. Black shows the upward-propagating secondary GWs, pink shows the initially-downward-propagating secondary GWs with $\lambda_H < 235$ km (which reflect upwards near the ground), and green shows the initially-downward-propagating secondary GWs with $\lambda_H > 235$ km (which reflect upwards in the mesosphere or lower thermosphere). The blue lines in b, d, f, and h show all of the secondary GWs combined. Panel B: Estimated 2D spectrum for all of the secondary GWs at the reflection altitude of z=240-290 km from b and d. From Vadas and Crowley (2009).

Histograms of secondary GWs

• Panel A of Fig. 11 shows the spectra for the identified secondary GWs propagating N/NWward at Wallops Island. Most of the GWs are medium-scale with $\lambda_H = 100 - 400$ km, have periods of $\tau_r \sim 15 - 25$ min and have horizontal phase speeds of $c_H \sim 150 - 200$ m/s.

• Panel B of Fig. 11 shows the 2D secondary GW spectrum at the reflection altitude. The spectrum peaks at $\lambda_H \sim \lambda_z \sim 150$ km, with a long tail extending to $\lambda_H \sim 2000$ km and $\lambda_z \sim 600$ km. Because this spectrum is ~ 100 km above the estimated source altitude, it has undergone substantial dissipative filtering, and so does not represent the true secondary GW "source" spectrum. Indeed, Vadas (2007) shows that dissipative filtering partially damps those secondary GWs with $\lambda_H \gtrsim 400-600$ km at these altitudes.

Conclusions

• TIDs were observed by TIDDBIT at Wallops Island on 30 October, 2007. This dataset provided an excellent opportunity to study the characteristics of secondary GWs, because the nearest deep convection S and SE of Wallops Island was ~ 2000 km away, which precludes primary GWs with periods as small as $15 - 25$ min.

• Most of the TIDs were propagating N/NWward, from the direction of TS Noel. Their wavelengths, phase speeds, and periods agree well with GW propagation and dissipation theory.

• This study confirms the likely existence of secondary GWs excited by thermospheric body forces, previously only postulated theoretically. 27 of the 33 N/NWward-propagating GWs were identified as secondary GWs from thermospheric body forces created by the intense convection in TS Noel. None were identified as primary convective GWs, because they reverse ray-traced ~ 500 km north of the nearest convective plumes. 21 of the secondary GWs were identified as likely initially downgoing, while 6 were identified as likely initially upgoing.

• At the bottomside of the F region at $z \sim 250$ km, the secondary GW spectrum peaks at $\lambda_H \sim 100 - 300$ km, $c_H = 100 - 300$ m/s, and $\tau_r \sim 15 - 25$ min. Medium-scale secondary waves with $\lambda_H \sim 100 - 400$ km are expected to be excited from thermospheric body forces theoretically, since these forces vary over horizontal scales of $100 - 300$ km (see Fig. 6).

• Secondary GWs are a thermospheric source of GWs, and can propagate up to $400 - 500$ km (Vadas, 2007), thereby extending the influence and ionospheric variability created by a single convective plume to very high altitudes. (Primary GWs can propagate no higher than ~ 300 km.) Additionally, secondary GWs propagate globally, further extending the influence and variability caused by a single convective plume.

• Because secondary GWs have scales as small as $\lambda_H = 100$ km and $\tau_r = 25 - 90$ min, have density perturbations of $\sim 5 - 15\%$ near the equator, and propagate within the F region, they may play a role in seeding ESF and plasma bubbles at the bottomside of the F layer.